Progress in Organic Coatings 172 (2022) 107067

Contents lists available at ScienceDirect

Progress in Organic Coatings

journal homepage: www.elsevier.com/locate/porgcoat

The influence of talc particles on corrosion protecting properties of polyurethane coating on carbon steel in 3.5 % NaCl solution

Elaheh Abil, Reza Arefinia *

Chemical Engineering Department, Faculty of Engineering, Ferdowsi University of Mashhad, Mashhad, Iran

ARTICLE INFO

Keywords:
Polyurethane
Talc
Anticorrosion
EIS
Wettability
Adhesion

ABSTRACT

In this study, the main concern is investigating the effect of talc on the protecting properties of polyurethane (PU) coating based on acrylic polyol/hexamethylene diisocyanate. To this end, PU coatings containing different concentrations of talc (0, 5, 10 and 15 %), were prepared and applied to the steel surface. Anticorrosion behavior of the coatings was evaluated by electrochemical impedance spectroscopy (EIS) during 90 days of immersion in 3.5 % NaCl. The EIS data were used to simulate the anticorrosion behavior of the coatings by using equivalent circuit models (ECMs). The obtained results showed the highly positive effect of talc and the best protective performance was obtained at 10 % by weight of talc concentration. Moreover, different complementary tests, including the surface study by scanning electron microscopy (SEM) and atomic force microscopy (AFM), wettability by contact angle and the coating adhesion by pull-off test were employed to satisfy the EIS data and further study the protecting behavior of PU coating, modified with talc particles.

1. Introduction

Organic coatings have been extensively used to protect the metal surface against corrosion in various environments [1,2]. Polyurethane (PU) due to its good properties such as high impact and abrasion resistance, chemical resistance, flexibility at low temperature, good UV resistance and color retention has been used in various coating applications [3–5]. Two-component systems of PU, obtained by the reaction between hydroxyl groups (polyol) and isocyanate groups (curing agent), are preferred because of their good flexibility in the formulation and the possibility of customization [6,7].

To improve the physical, mechanical and anticorrosion properties of PU coatings, researchers have studied the effect of a wide range of pigments such as graphene [8,9], titanium dioxide [10,11], and silica [12,13]. In view of anticorrosion property, it has been reported that some pigments such as: micaceous iron oxide (MIO), titanium dioxide (TiO_2), mica and talc (hydrated magnesium silicate) can improve the coating resistance by the barrier mechanism [14–16].

Talc is a natural mineral with the chemical formula $Mg_3Si_4O_{10}(OH)_2$ in a three-layer structure, composed of a hydroxide layer ($MgO{\cdot}H_2O$), placed between two silicate layers (SiO_2) [17,18]. Talc is commonly incorporated in organic coatings in order to: reduce the cost as an extender, improve the mechanical properties such as hardness and abrasion resistance [19,20] and create better thermal properties, including thermal stability and flame retardancy [19,21]. Moreover, it has been reported that talc particles, in combination with the epoxy and sol–gel coatings [22,23], could improve the barrier property against the corrosion process by the plate-like shape [24]. However, the effect of talcum powder on the anticorrosion behavior of the PU coating has not been investigated, yet.

The aim of this work is to study the effect of talc concentration on the anticorrosion behavior of the PU coating applied to the carbon steel surface in 3.5 % NaCl solution by electrochemical impedance spectroscopy (EIS). The protection property was further investigated by different complementary tests including the surface analysis methods of scanning electron microscopy (SEM) and atomic force microscopy (AFM), the contact angle measurement and the adhesion test of pull-off.

2. Experimental

2.1. Materials and coating preparation

Solvent based acrylic polyol as a resin with solid content with 65 % along with 4.5 % hydroxyl functionality was purchased from Taak resin Kaveh Co. and micro size talc pigments were procured from Hunan chemical Co. An aliphatic polyisocyanate curing agent, hexamethylene

* Corresponding author at: Department of Chemical Engineering, Faculty of Engineering, Ferdowsi University of Mashhad, Iran.
E-mail address: arefinia@um.ac.ir (R. Arefinia).

https://doi.org/10.1016/j.porgcoat.2022.107067
Received 15 April 2022; Received in revised form 22 July 2022; Accepted 24 July 2022

diisocyanate (HDI, Desmodur N75, NCO content 16.5 % and solid content 75 %) was purchased from Bayer Co., China.

To formulate the talc/PU coatings, in the first step, different concentrations (0, 5, 10 and 15 % by weight, based on the total solid content) of talc were gradually mixed with 30 g resin using a laboratory mechanical mixer for about 2 h to obtain a uniform suspension. In the second step, the curing agent at NCO:OH molar ratio of 1.2:1 was added to the talc/resin suspension and stirred for about 10 min. In this stage, the curing reaction is processed by the reaction between isocyanate and hydroxyl groups, leading to the formation of urethane group as shown in Fig. 1.

Before applying the coatings, the steel plates (St-37, from Foolad Mobarakeh Co.) with dimensions 2 mm × 7 cm × 7 cm, were polished with abrasive papers from grade 120 to 1200, degreased in acetone, rinsed with deionized water, and immediately dried with warm air. The talc/PU coatings were applied to the steel plates by using an air spray gun. The coated plates were left at room temperature (25 ± 2 °C) for 24 h; then, post-cured in an oven at 60 °C for 24 h. The average thickness of the dried coatings was 60 ± 5 μm. The talc/PU coatings containing different concentrations of talc are named in Table 1.

2.2. Pigment characterization

The crystalline structure of talc was investigated by X-ray diffraction (XRD, Explorer, GNR, Italy) with Cu Kα radiation ($\lambda = 1.5406$ Å, 40 kV, 30 mA) over a range of 3° to 50°. The d-spacing (interlayer distance) between the talc layers was determined using Bragg's law ($\lambda = 2d \sin\theta$) where λ corresponds to the wavelength of the X-rays and θ is the diffraction angle. Fourier-transform infrared (FTIR, Thermo Nicolet, Avatar 370, USA) was used to determine the functional groups of talc pigment. The analysis was performed with KBr pellets in the range of 4000–400 cm^{-1} with a resolution of 4 cm^{-1}.

The morphology and particle size of the talc powder were studied using the scanning electron microscope (SEM, LEO 1450VP, Zeiss, Germany).

2.3. Coating characterization

The electrochemical cell was made by a glassy tube, firmly attached to the coated steel panels where the isolated surface was about 9 cm^2 and the cell was filled with 65 ml of 3.5 % NaCl solution. The EIS measurements were carried out by an Autolab potentiostat/galvanostat 302N in a glassy electrochemical cell, including three-electrode cells: a saturated calomel electrode (SCE) and a graphite rod as a reference and auxiliary electrodes, respectively, and the working electrode was the steel plate surface, isolated by the glassy cell.

The EIS tests were conducted over a frequency range from 100 kHz to 10 mHz and at an amplitude perturbation of ±10 mV versus OCP until 90 days in different immersion intervals at room temperature. Before the EIS measurement, open circuit potential (OCP) was checked to be a constant value, indicating the steady state condition.

Measurement of contact angle was performed using a contact angle measuring system (SCAM, Adeeco, Iran) to check the wettability of the coatings surface. This test was carried out by dropping 5 μL of deionized water at two random regions of the coatings surface at room temperature.

Table 1
The talc/PU coatings with different concentrations of talc.

Talc concentration (% w/w)	Coating name
0	PUTa0
5	PUTa5
10	PUTa10
15	PUTa15

The morphology of the coatings surface was studied using SEM and atomic force microscope (AFM, ARA-AFM, Ara research, Iran). AFM was done using the tapping mode with the scan rate of 1 Hz and a tip radius of 10 nm. To measure the surface roughness, AFM images were analyzed by the software of Imager (provided by Ara research Co., version 1.00) on 10 μm × 10 μm imaged surface area.

The adhesion between the metal and coatings surface was measured by an Elcometer 508 digital pull-off adhesion tester (Elcometer, UK). To this end, a 20 mm diameter dolly was firmly glued to the coatings surface using a cyanoacrylate adhesive (MC1500 commercial name) at room temperature.

3. Results and discussion

3.1. Characterization and dispersion of talc particles

The morphology of talc particles was examined by SEM analysis and the taken image is shown in Fig. 2. It is obvious that talc pigments have an irregular-platy shape, as addressed by other researchers [24,25]. Dimensions of talc particles were inspected by ImageJ software and the statistical analysis of various SEM images showed a relatively narrow size distribution where width and length of particles are nearly the same (4.1 ± 0.6 μm), and the average thickness is 550 ± 40 nm.

The chemical structure of talc was characterized by FTIR and the recorded spectrum is shown in Fig. 3. The characteristic peaks at 3676 cm^{-1} and 3423 cm^{-1} correspond to the vibrations of Mg-OH and Si-OH

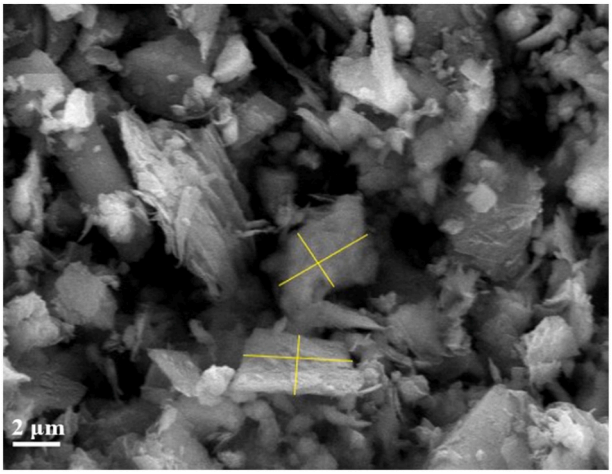

Fig. 2. SEM image of talc pigments.

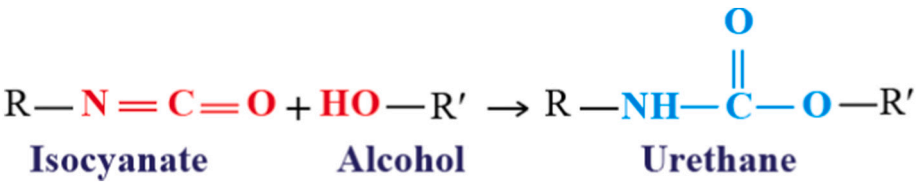

Fig. 1. A simplified reaction scheme for the formation of polyurethane.

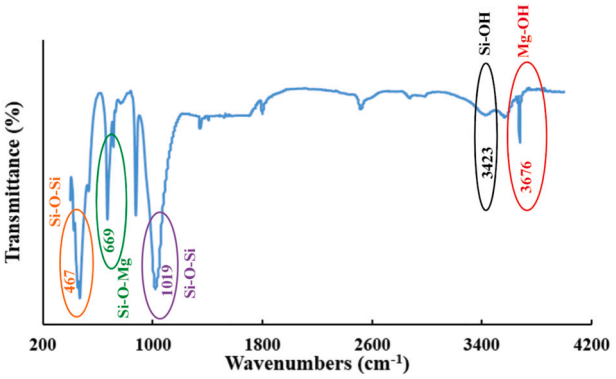

Fig. 3. FTIR spectrum of talc powder.

groups, respectively [26,27]. Both bands at 467 cm^{-1} and 1019 cm^{-1} reflect the stretching vibration of Si-O-Si, which confirms the existence of a SiO_4 tetrahedral layer in the crystal structure of talc [28,29]. While the peak at 669 cm^{-1} corresponds to the coupling layers band (Si-O-Mg) [27].

Fig. 4 shows the XRD pattern of talc powder, PUTa10 and PUTa15 coatings. The presence of two main peaks at 9.48° and 28.64° are attributed to the crystalline structure of talc ($Mg_3Si_4O_{12}H_2$) which is in agreement with those obtained elsewhere [30–32]. The basic structure of talc consists of a magnesium hydroxide layer sandwiched between two silica layers [33–35]. The sharp peak, appeared at 2θ = 9.48°, corresponds to d-spacing of about 9.32 Å (determined using Bragg's law) [36]. In the case of PUTa10 coating, this peak disappears from the XRD pattern, indicating the good dispersion of talc particles within the coating. However, in the case of PUTa15, a weak diffraction peak at 2θ = 9.48° can be attributed to the agglomeration of talc particles, which will be further investigated by the surface analysis methods. For both PUTa10 and PUTa15 coatings, there is a broad peak at 2θ = 19.3°, which is ascribed to the amorphous feature of the cross-linked polymer matrix [5].

3.2. EIS measurements

3.2.1. Corrosion performance of the coated samples

For PU coatings containing different concentrations (0, 5, 10 and 15 % by weight) of talc, EIS test was performed during 90 days of immersion in 3.5 % NaCl solution at room temperature. The obtained data in the forms of Nyquist and the Bode plots are typically shown in Fig. 5. The shape of the Nyquist plots helps to select a suitable equivalent circuit model (ECM) to simulate the anticorrosion behavior of the coatings.

In this regard, Fig. 5 shows two different shapes of the Nyquist diagrams: at early times of immersion, the Nyquist plots for PUTa5 (Fig. 5c) and PUTa10 (Fig. 5e) are as one semi-circle, indicating the intact state of coatings; i.e., the corrosion rate at the metal surface is negligible [1,37,38]. In this situation, the ECM with one circle (Fig. 6a) is frequently applied to simulate the anticorrosion behavior of coatings. In this model, R_s and R_{pore} are attributed to the solution and the pore resistance, respectively. The element of CPE_c denotes the constant phase element (CPE) of a coating, frequently used to better fit the impedance data when a deviation from the ideal capacitance behavior exists due to the inhomogeneity or porosity [1,2]. The impedance of a CPE is defined as:

$$Z_{CPE} = (Y(j\omega)^n)^{-1} \quad (1)$$

where Y is the CPE constant with a dimension of Ω^{-1} s^n cm^{-2}, j is the imaginary number ($\sqrt{-1}$), ω and n are the angular frequency (rad/s) and CPE exponent (as a measure of the surface inhomogeneity or porosity level), respectively.

The value of ideal capacitance of coating (C_c, measures the amount of water uptake in the barrier coatings [39]) can be calculated using the CPE parameters using Hsu and Mansfeld formula as following [40,41]:

$$C_c = \left(Y_c / R_{pore}^{n_c - 1}\right)^{1/n_c} \quad (2)$$

where parameters n_c and Y_c are the CPE exponent and constant of a coating, respectively.

After the intact stage, appearance of the additional part at the low frequencies (see Fig. 5) indicates that the corrosion rate is significant because of the high diffusion rate of corrosive species such as water and chloride ions to the metal surface. In this situation, the anticorrosion state of coatings is commonly called as a defected state [42,43]. Considering the above concepts, Fig. 5 shows that PUTa0 and PUTa15 coatings have a defected state approximately from the initial time of immersion, while it can be observed for PUTa5 and PUTa10 coatings after 5 and 7 days, respectively. These evidences, qualitatively suggests the better protection of the PU coating with 10 % talc concentration. However, the simulation of coatings performance by using ECMs also helps to quantitatively study the effective impedance parameters and determine the predominant protection mechanism, during immersion time. In addition, it is necessary to inspect the coating behavior by EIS in long term to guarantee a reliable protection behavior.

Moreover, the straight-line shape of the second part in the Nyquist plots advises that the corrosion process is mainly controlled by the diffusion mechanism. This can be described by the fact that talc particles, incorporated in the coating structure, act as a barrier to the penetration of corrosive ions.

In the case of a defected coating, the ECM shown in Fig. 6b, is often used to simulate the protective behavior. In this ECM, the element of CPE_{dl} is attributed to CPE of a double layer and hence the ideal value of the double layer capacitance (C_{dl}) can be calculated by Eq. (2), at which n_{dl} and Y_{dl} are used as the CPE exponent and constant for the double layer, respectively. The elements Z_D and R_{ct}, shown in Fig. 6b, are attributed to the diffusion phenomenon and charge transfer resistance, respectively. However, in the present work, the corrosion process occurs under a diffusion controlling mechanism, and hence, the value of R_{ct} is negligible compared to the diffusion impedance. The impedance of element Z_D, considering Fick's *second* law of diffusion, is defined by the following relation [44]:

$$Z_D = \frac{R_w tanh\left[(T\omega j)^{0.5}\right]}{(T\omega j)^{0.5}} \quad (3)$$

where R_w corresponds to the diffusion resistance, T (sec) is the time constant.

The EIS spectra were well fitted by using the ECMs (shown in Fig. 6) in Zview software and the impedance parameters for both the coating structure and double layer during 90 days of immersion were extracted

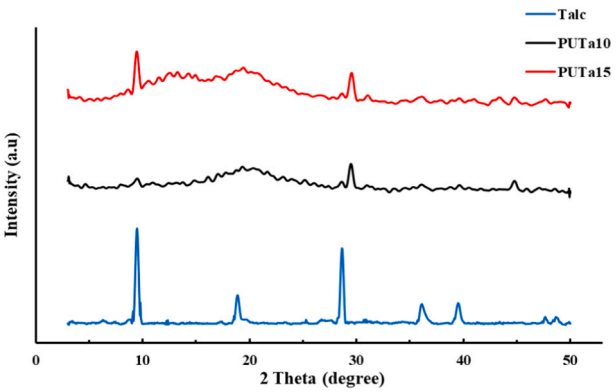

Fig. 4. XRD pattern of talc powder, PUTa10 and PUTa15 coatings.

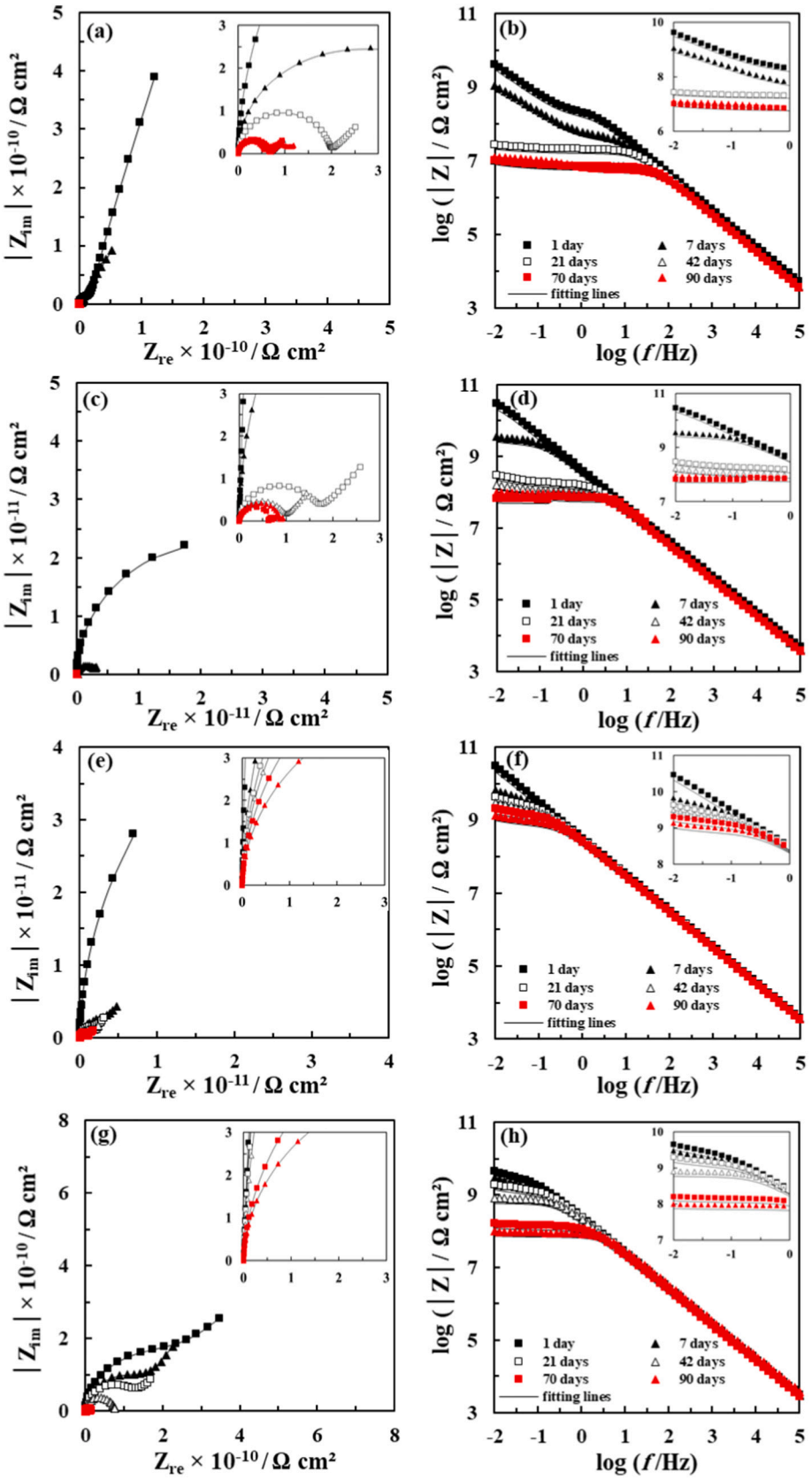

Fig. 5. Nyquist and Bode module plots versus time for different PU coatings: (a and b) PUTa0, (c and d) PUTa5, (e and f) PUTa10, (g and h) PUTa15 in 3.5 % NaCl solution.

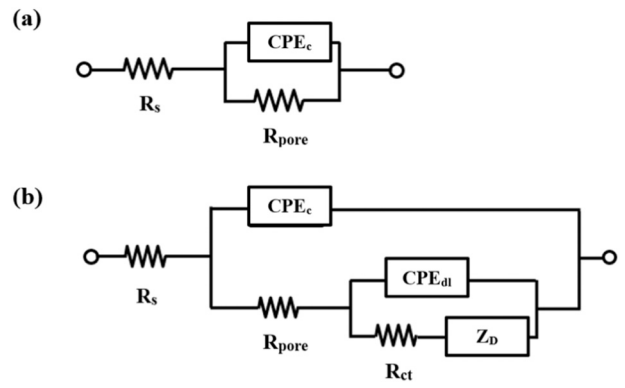

Fig. 6. ECMs used for the analysis of EIS data.

and will be discussed in the following sections.

3.2.2. Coating impedance parameters

The variations of the coating impedance parameters versus immersion time at different concentrations of talc are presented in Fig. 7. It can be seen from Fig. 7a, that the pore resistance (R_{pore}) for all talc concentrations decreases, where the rate of reduction is more significant at the initial period of immersion. This can be related to the change in the anticorrosion state from an intact to a defected coating. After a specific time of immersion, the R_{pore} values become approximately constant, suggesting the steady state of corrosion.

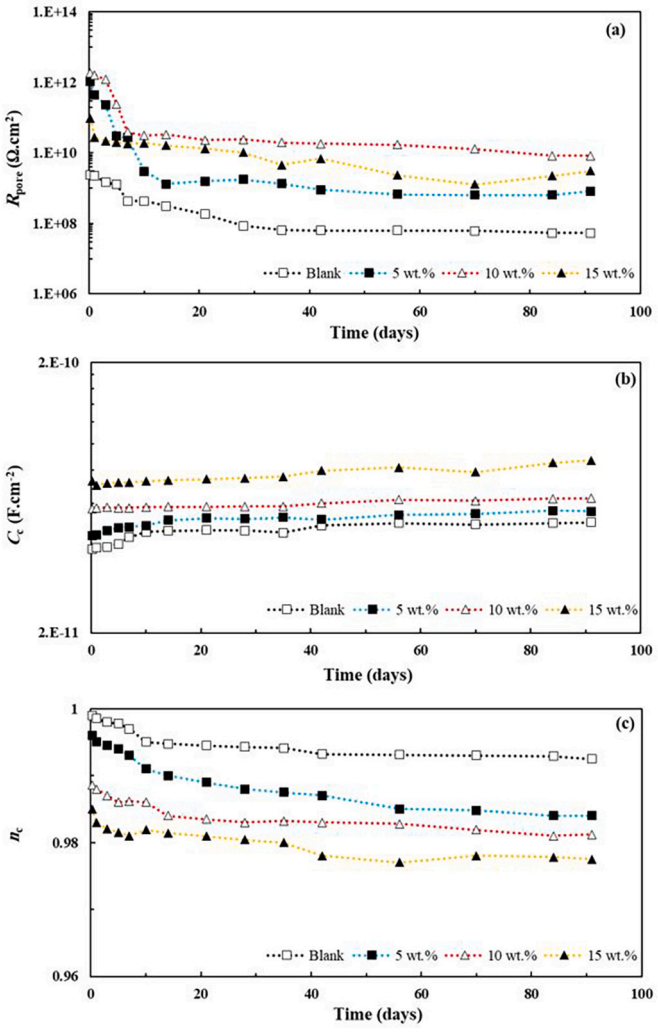

Fig. 7. The time dependency of coating impedance parameters: (a) R_{pore}, (b) C_c and (c) n_c at different concentrations of talc in 3.5 % NaCl solution.

Generally, Fig. 7a shows that the value of R_{pore} increases with the sequence: PUTa10 > PUTa15 > PUTa5 ≫ PUTa0. This trend of variations indicates the highly positive influence of talc particles on the protection strength of PU coating against the corrosion process, as reported previously for other coatings [22,23]. Improvement of the coating resistance in the presence of talc particles can be explained by the platy shape of talc particles (Fig. 2), which improves the barrier properties of PU coatings. Indeed, talc platelets act as a physical barrier to the diffusion of water and chloride ions, forcing them to travel through a winding path in the coating thickness to reach the metal surface [45,46]. However, the highest value of coating resistance (about $10^{10}\Omega.cm^2$) is obtained by incorporating 10 % by weight of talc concentration. When talc concentration increases from 10 to 15 %, the value of R_{pore} decreases, likely due to agglomeration of talc particles, as noted by XRD pattern (Fig. 4). This facilitates the diffusion of electrolyte species towards the metal surface [19].

Fig. 7b shows the time dependency of coating capacity, C_c, at different talc concentrations. For all coatings, the value of C_c increases with time, due to the enhancement of water content within the coating structure over the immersion time. This phenomenon has been well addressed by the penetration phenomenon of water molecules through the micropores of a coating, causing the increase of C_c value due to the high value of dielectric constant for water ($\varepsilon = 80$) [2,22]. This trend of variation for C_c is in good agreement with that observed for R_{pore} (Fig. 7a), i.e., the reduction of coating resistance facilitates the diffusion of water molecules and hence the C_c value increases.

Moreover, Fig. 7b shows that for all times, C_c values has a direct dependency with talc concentration, which is different from that obtained by R_{pore} for when talc concentration increases from 0 to 10 %. In other words, for a coating with the conventional barrier mechanism, it is expected the decrease of C_c of with the increase of R_{pore} due to the lower penetration of water in the coating structure. This contradiction can be explained by the fact that from one hand, C_c value is directly proportional to the dielectric constant (ε); on the other hand, the value of ε for talc (≈9.4) is greater than that for a neat PU coating (≈5.8) [47,48]. Thus, the increase of C_c with talc concentration is reasonable due to the predominant effect of dielectric constant of talc compared to penetration of water. However, for the talc concentration >10 %, both the water penetration and the increment of talc content cause the increase of the coating capacitance.

Moreover, the volume fraction of water absorbed (V_w) within the coating structure can be directly calculated with Brasher and Kingsbury equation [49]:

$$V_w = \frac{log\left(C_t/C_0\right)}{log\varepsilon_w} \quad (4)$$

where C_0 and C_t are coating capacitance at the initial time of immersion and the arbitrary time of t, respectively. The parameter ε_w denotes the dielectric constant of water. Fig. 8 shows variation of V_w versus talc concentration at different immersion times.

As can be seen, for all talc concentrations, V_w is increased with immersion time. Moreover, the amount of water, absorbed within the coating structure, increases when talc concentration increases up to 10 %; however, further addition of talc particles causes the increase of V_w. These behaviors can be directly related to the barrier property of PU coatings against water penetration through the micropores, described in term of R_{pore}.

The variations of n_c with time for all PU coatings are presented in Fig. 7c. Accordingly, parameter n_c is decreased by increasing both the talc concentration and the immersion time. The effect of talc concentration can be attributed to its superficial heterogeneity, arisen from the rigid structure and the chemical composition of talc [25,34]. While the

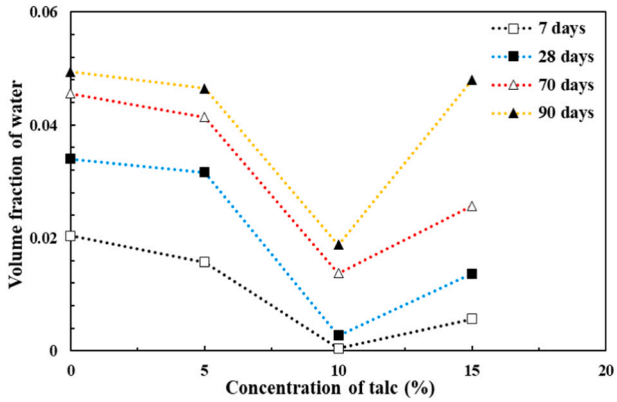

Fig. 8. Effect of talc concentration on the volume fraction of water absorbed (V_w) by PU coatings at different immersion times.

effect of immersion time can be related to the increase of coating porosity as discussed before in the case of R_{pore} parameter.

3.2.3. Corrosion impedance parameters

The time dependency of the corrosion impedance parameters for PU coatings with different concentrations of talc powder is shown in Fig. 9.

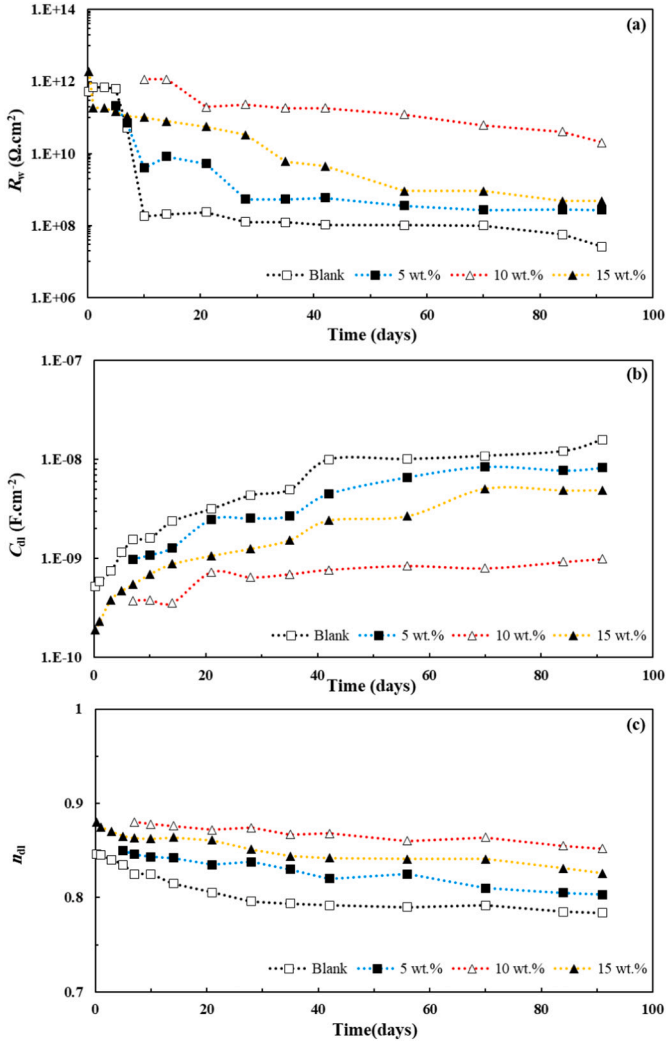

Fig. 9. The time dependency of double layer parameters: (a) R_w, (b) C_{dl}, (c) n_{dl} at different concentrations of talc in 3.5 % NaCl solution.

After an initial period of immersion, diffusion resistance (R_w) for all coatings (except PUTa10) is intensively decreased and then has no significant change up to the end of immersion. It can be found that the final value of R_w is proportional to the initial period of immersion; i.e., the greater initial period of immersion, the higher final value of R_w.

Considering the final values of R_w, the effect of talc concentration is in the following order: PUTa10 ≫ PUTa15 > PUTa5 > PUTa0, which is in keeping with that obtained for R_{pore} (Fig. 7) and reported previously [1]. It can be assumed that the blending of rigid talc particles with soft PU binder provides a physical barrier within the diffusion pathway of corrosive species (water and chloride ions) towards the metal surface [23]. In the case of PUTa10 coating, the highest value of R_w (in order of 10^{10} Ω.cm^2) is obtained and remains approximately constant during immersion time, confirming the best performance of PU coating at 10 % talc concentration.

Fig. 9b shows that for all PU coatings, the value of C_{dl} is continuously increased with immersion time which is probably arisen from the increase of water molecules in the metal/coating interface [50–52], due to the reduction of diffusion resistance of coatings, R_w (Fig. 9a). In this regard, the electrolyte penetration causes the formation of a double layer in the disbonded area of metal/coating interface and hence the corrosion process is developed [53]. It can be suggested that C_{dl} is a measure of both the underlaying area at which the coatings are damaged and the amounts of water molecules penetrated in the double layer [50]. Moreover, Fig. 9b shows that the effect of talc concentration on the C_{dl} value is in agreement with that obtained for R_w, where PUTa10 and PUTa0 coatings have the lowest and the highest values of C_{dl}, respectively.

As shown in Fig. 9c, the value of n_{dl} for all coatings decreases during the immersion time, probably due to the accumulation of corrosion products, causing a higher level of heterogeneity in the metal/coating interface [2]. Moreover, the effect of talc concentration on the parameter n_{dl} depends on the values of R_{pore} and R_w; i.e., the increase of coating and diffusion resistance causes a reduction in the corrosion rate and hence the value of n_{dl} increases.

3.3. Surface analysis of coatings

Before immersion, the surface of PU coatings, modified with different talc concentrations, was studied using SEM and AFM and the taken images are shown in Fig. 10. As can be seen from SEM images, the surface of PUTa0 (Fig. 10a) is black and uniform, while the existence of white regions on the other coatings corresponds to the presence of talc particles, where these regions become larger by increasing the talc concentration. Moreover, SEM images show that the non-homogeneity of the coatings surface increases with talc concentration and even for PUTa15 coating, the agglomeration of talc particles is obvious (Fig. 10d). This can be assumed as the main reason for the significant reduction of R_{pore} at 15 % talc concentration as mentioned by EIS data (Fig. 7a).

Moreover, the surface morphology of PU coatings was inspected by AFM and the values of average roughness (R_a) are presented in Fig. 10b, d, f, and h. Taken into account the values of R_a, the increase of talc concentration causes the higher roughness of PU coatings. This finding along with the SEM observations explain the reduction of parameter n_c by the increase of talc concentration (Fig. 7c).

After 90 days of immersion in 3.5 % NaCl solution, the surface analysis of PU coatings was performed by SEM and the micrographs are shown in Fig. 11. The presence of crack at the surface of PUTa0 coating (Fig. 11a), reflects the deterioration of this coating during 90 days immersion as reported by the low value of pore resistance (R_{pore}). However, in the case of other coatings, blending with talc particles (Fig. 11b up to c), no severe damage can be detected. This evidence confirms the positive effect of talc particles on the protective behavior of PU coating during 90 days immersion in 3.5 % NaCl solution. The high level of heterogeneity at the surface of PUTa15 (Fig. 11d) is likely arisen from its

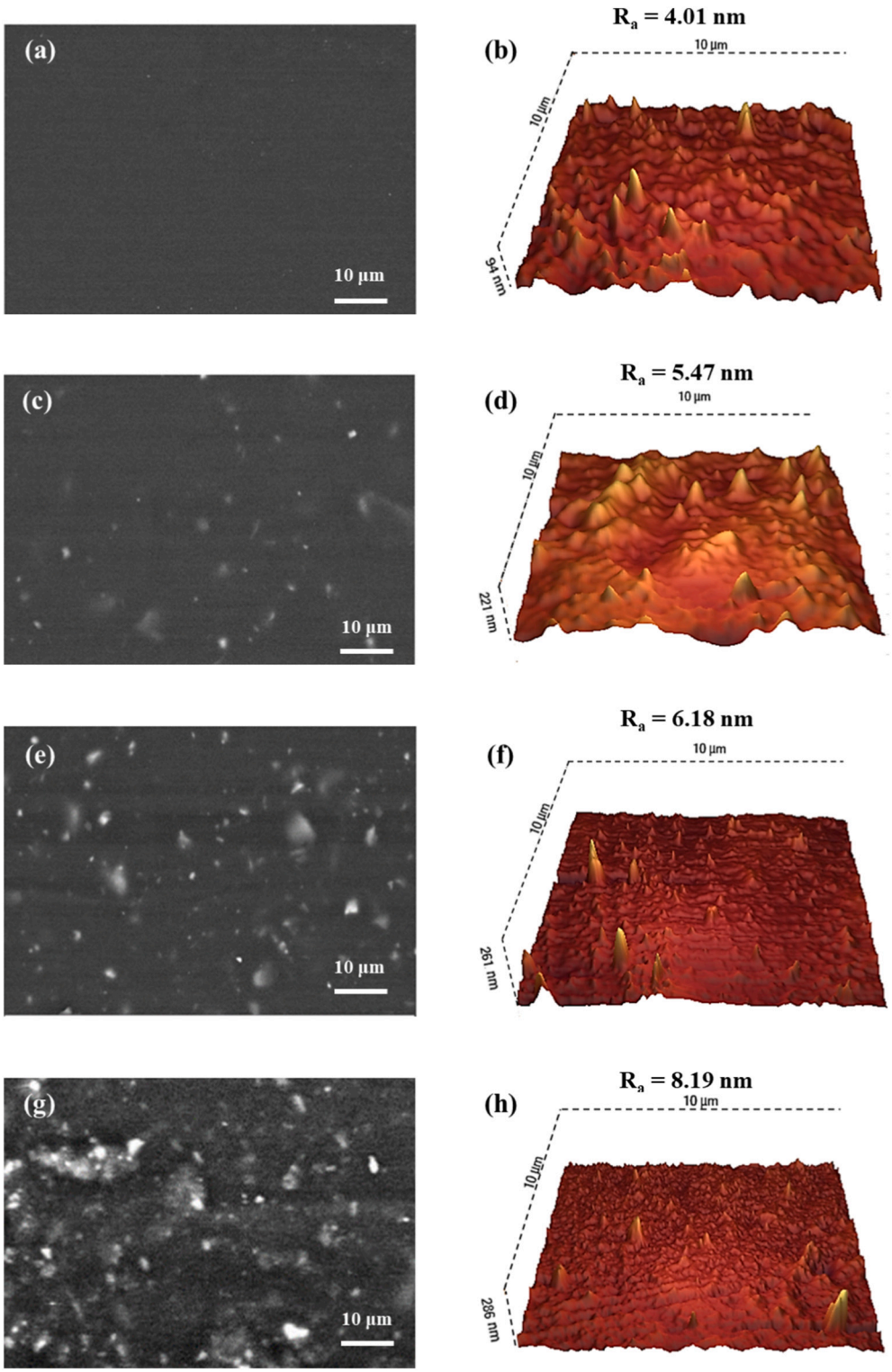

Fig. 10. SEM and AFM images taken at the surface of different PU coatings: (a and b) PUTa0, (c and d) PUTa5, (e and f) PUTa10 and (g and h) PUTa15, before immersion.

porous structure, allowing the electrolyte penetration within the coating structure.

3.4. Surface wettabillity

The contact angle of PU coatings is measured and presented in Fig. 12. The values of contact angle for PU coatings, modified with talc particles, are higher than that for PUTa0 coating, indicating the normal hydrophobicity of PU coating in the presence of talc. It is well known that talc has the hydrophobic property (with a contact angle approximately >90° [54]) due to the tetrahedral siloxane (–Si–O–Si–) surface in the basal cleavage face, which is analyzed by FTIR (Fig. 3) and occupies approximately 90 % of the talc surface [55,56]. However, the edge face of talc is hydrophilic, due to the presence of MgOH and SiOH groups

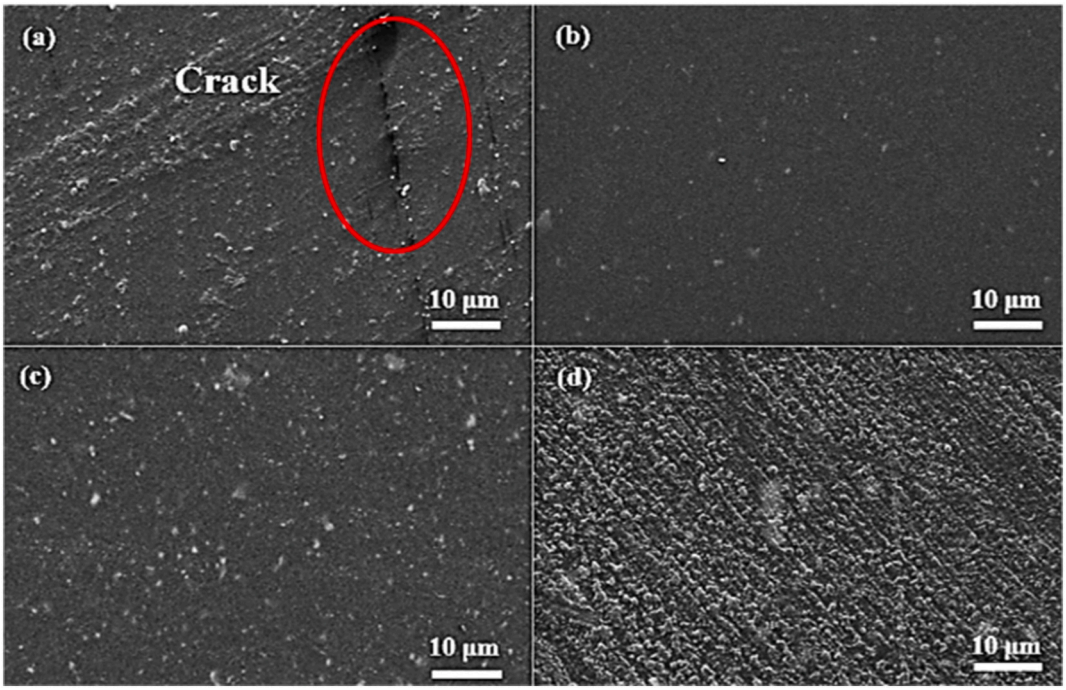

Fig. 11. SEM images taken at the surface of different PU coatings: (a) PUTa0, (b) PUTa5, (c) PUTa10 and (d) PUTa15, after 90 days immersion in 3.5 % NaCl solution.

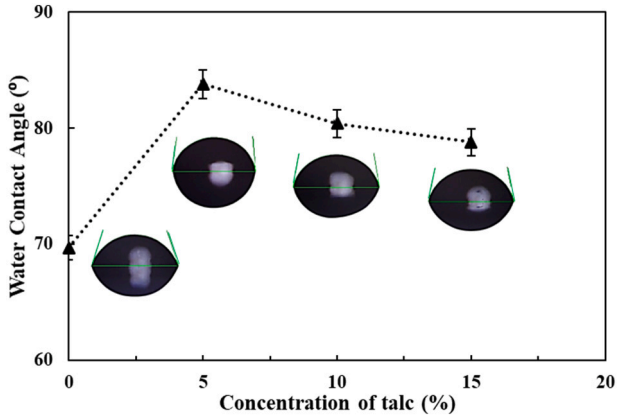

Fig. 12. Effect of talc concentration on the contact angle of PU coating.

[55,57,58] as noticed in the FTIR analysis.

The highest value of contact angle (83.8°) is obtained at 5 % talc, while further incorporation of talc powder up to 15 % causes a decrease in the value of contact angle. This behavior can be explained by the fact that the increase of talc concentration is associated with two opposite effects: from one hand, the increment of hydrophobic property due to the intrinsic nature of talc; on the other hand, the increase of wettability because of the increase in the surface roughness of PU coatings (as obtained by AFM in Fig. 10) and well stated by Wenzel equation [59]. Therefore, it can be concluded that the later effect is dominant for PU coatings modified with talc particles.

Considering the contact angle and EIS results, it can be assumed that wettability has no significant effect on the corrosion protection of PU coatings when talc concentration changes from 5 to 15 %. However, this effect can be more pronounced for PU coating in the presence of talc particles compared to the neat PU coating, because of the higher difference between the contact angle values.

3.5. Pull-off adhesion test

The interfacial adhesion between carbon steel and PU coating at different concentrations of talc particles, both before and after 20 days of immersion in 3.5 % NaCl solution, was studied using the pull-off test and the obtained results are given in Table 2.

It is expected that the urethane bonds can enhance the coating adhesion to the metal surface [60,61]. While, the values of adhesive strength in the presence of talc, both before and after immersion, are much greater than that of in the absence of talc (PUTa0). Before immersion, when the talc concentration increases up to 15 %, the adhesive strength increases continuously from 2.7 to 9.1 MPa, indicating talc powder could improve the coating adhesion to the metal substrate as reported elsewhere [18,62]. It was proposed that at the low concentrations of talc (<5 %), the increase of both coating cohesion and mechanical interlocking are the main reasons for the better adhesion [62,63]. While, at the high level of talc concentrations (>5 %), the adhesion of coating to the substrate is improved by the reduction in the shrinkage of coating during the curing process [21,64]. Therefore, it can be assumed that both mechanisms (at low and high concentrations of talc) can be effective in the present work.

From Table 2, it is evident that after immersion, the highest value of adhesive strength is obtained at 10 % concentration of talc, which is consistent with the best anticorrosion properties of PUTa10 coating. More inspection reveals that after immersion, the trend of variations of adhesive strength with talc concentration is inverse to that obtained for parameter C_{dl} (Fig. 9b), i.e., the higher adhesive strength, the lower C_{dl}

Table 2
Pull-off test for PU coatings at different talc concentrations before and after 20 days of exposure to 3.5 % NaCl solution.

Average value of pull-off strength (MPa)	PUTa0	PUTa5	PUTa10	PUTa15
Before immersion	2.7 ± 0.3	6.5 ± 0.2	7.5 ± 0.4	9.1 ± 0.3
After 20 days immersion	2.0 ± 0.2	3.8 ± 0.3	7.3 ± 0.3	6.1 ± 0.2

value. This confirms that the increase of adhesion between the metal and coating surface causes a decrease in the disbonding area of the coating/metal interface.

4. Conclusions

In this work, the effect of talc concentration on the corrosion protection behavior of PU coating, applied to the steel surface was carefully investigated using EIS and different complementary tests, during 90 days of immersion in 3.5 % NaCl solution. The most important results are summarized as follows:

- The incorporation of talc particles significantly improves the protection properties of PU coating, compared to PU coating without talc. The corrosion process was mainly controlled by a diffusion mechanism, attributed to the barrier effect of talc particles within the coating structure. The EIS results showed that an increase in talc concentration from 0 to 10 % is associated with the increase of both pore resistance (R_{pore}) and diffusion resistance (R_w), due to the creating indirect pathways for the penetration of electrolyte species within the coating structure as a result of the platy shape of talc particles. However, further addition of talc causes a negative effect on the barrier property of PU coatings mainly due to the agglomeration process.
- The contact angle measurement suggests the normal hydrophobic property of PU coatings, modified with talc particles, compared to the PU coating without talc. However, it can be found that the hydrophobicity of talc particle has a minor effect on the barrier properties.
- The adhesion of PU coating to the metal surface significantly increases by talc concentration; however, after immersion in the electrolyte, the highest adhesive strength corresponds to the PU coating with 10 % by weight of talc concentration. These findings are consistent with the variations of parameter C_{dl}. In other words, the disbonding phenomenon of PU coatings is directly proportional to the adhesive strength of coatings to the metal substrate.
- It can be concluded that talc particles can improve the barrier property of PU coating through two main effects: (a) the increase of diffusion pathways, mainly due to the platy structure of talc particles and (b) the higher adhesion of PU coating to the metal surface and hence the reduction of coating disbonding. Although, the hydrophobic property of PU coatings in the presence of talc particles have also a minor effect on the barrier property.

CRediT authorship contribution statement

We the undersigned declare that this manuscript is original, has not been published before and is not currently being considered for publication elsewhere.

We confirm that the manuscript has been read and approved by all named authors and that there are no other persons who satisfied the criteria for authorship but are not listed. We further confirm that the order of authors listed in the manuscript has been approved by all of us.

We understand that the Corresponding Author is the sole contact for the Editorial process. He/she is responsible for communicating with the other authors about progress, submissions of revisions and final approval of proofs.

Declaration of competing interest

The authors whose names are listed immediately below certify that they have NO affiliations with or involvement in any organization or entity with any financial interest (such as honoraria; educational grants; participation in speakers' bureaus; membership, employment, consultancies, stock ownership, or other equity interest; and expert testimony or patent-licensing arrangements), or non-financial interest (such as personal or professional relationships, affiliations, knowledge or beliefs) in the subject matter or materials discussed in this manuscript.

Data availability

No data was used for the research described in the article.

References

[1] R. Arefinia, A. Shojaei, H. Shariatpanahi, J. Neshati, Anticorrosion properties of smart coating based on polyaniline nanoparticles/epoxy-ester system, Prog. Org. Coat. 75 (2012) 502–508.
[2] M. Rayati, R. Arefinia, Anticorrosion behavior of DBSA doped polyaniline nanoparticles/epoxy ester coating on carbon steel in saline-alkaline solution, Prog. Org. Coat. 105451 (2020).
[3] D. Chattopadhyay, R.V. Kothapalli, Structural engineering of polyurethane coatings for high performance applications, Prog. Polym. Sci. 32 (2007) 352–418.
[4] J.H. Li, R.Y. Hong, M.Y. Li, H.Z. Li, Y. Zheng, J. Ding, Effects of ZnO nanoparticles on the mechanical and antibacterial properties of polyurethane coatings, Prog. Org. Coat. 64 (2009) 504–509.
[5] B. Yu, X. Wang, W. Xing, H. Yang, L. Song, Y. Hu, UV-curable functionalized graphene oxide/polyurethane acrylate nanocomposite coatings with enhanced thermal stability and mechanical properties, Ind. Eng. Chem. Res. 51 (2012) 14629–14636.
[6] Z.S. Petrović, J. Ferguson, Polyurethane elastomers, Prog. Polym. Sci. 16 (1991) 695–836.
[7] V.M. Mannari, J.L. Massingill, Two-component high-solid polyurethane coating systems based on soy polyols, JCT Res. 3 (2006) 151–157.
[8] P. Haghdadeh, M. Ghaffari, B. Ramezanzadeh, G. Bahlakeh, M.R. Saeb, The role of functionalized graphene oxide on the mechanical and anti-corrosion properties of polyurethane coating, J. Taiwan Inst. Chem. Eng. 86 (2018) 199–212.
[9] S. Habibpour, J.G. Um, Y.-S. Jun, P. Bhargava, C.B. Park, A. Yu, Structural impact of graphene nanoribbon on mechanical properties and anti-corrosion performance of polyurethane nanocomposites, Chem. Eng. J. 405 (2021), 126858.
[10] J. Kasanen, M. Suvanto, T.T. Pakkanen, UV stability of polyurethane binding agent on multilayer photocatalytic TiO2 coating, Polym. Test. 30 (2011) 381–389.
[11] M. Taheran, A.H. Navarchian, R.S. Razavi, Optimization of wear resistance of PU/TiO2 coatings on aluminum surfaces, Prog. Org. Coat. 72 (2011) 486–491.
[12] A.P. Kabra, P. Mahanwar, V. Shertukde, V. Bambole, Performance of nanosilica in acrylic polyol 2K polyurethane coatings, Pigment. Resin Technol. 41 (2012) 230–239.
[13] F. Carreño, M.R. Gude, S. Calvo, O. Rodríguez de la Fuente, N. Carmona, Synthesis and characterization of superhydrophobic surfaces prepared from silica and alumina nanoparticles on a polyurethane polymer matrix, Prog. Org. Coat. 135 (2019) 205–212.
[14] A. Mishra, R. Narayan, R.V. Kothapalli, T. Aminabhavi, Hyperbranched polyurethane (HBPU)-urea and HBPU-imide coatings: effect of chain extender and NCO/OH ratio on their properties, Prog. Org. Coat. 74 (2012) 134–141.
[15] G. Reinhard, Formulation of water-borne dispersions for corrosion-protective primers, Prog. Org. Coat. 18 (1990) 123–145.
[16] V. Mannari, C.J. Patel, Understanding Coatings Raw Materials, Vincentz Network, 2015.
[17] V. Wallqvist, P.M. Claesson, A. Swerin, J. Schoelkopf, P.A.C. Gane, Interaction forces between talc and hydrophobic particles probed by AFM, Colloids Surf. A Physicochem. Eng. Asp. 277 (2006) 183–190.
[18] A. Kalendová, D. Veselý, P. Kalenda, Properties of paints with hematite coated muscovite and talc particles, Appl. Clay Sci. 48 (2010) 581–588.
[19] X.Y. Sun, J.L. Kang, J.Z. Hang, L.J. Jin, F. Xu, L.Y. Shi, Preparation and characterization of uv-curable talc/acrylate composite coatings with enhanced flame-retardancy, Adv. Mater. Res. 750–752 (2013) 2057–2062.
[20] J.K. Katiyar, S.K. Sinha, A. Kumar, Friction and wear durability study of epoxy-based polymer (SU-8) composite coatings with talc and graphite as fillers, Wear 362 (2016) 199–208.
[21] H.H. Dzulkafli, F. Ahmad, S. Ullah, P. Hussain, O. Mamat, P.S. Megat-Yusoff, Effects of talc on fire retarding, thermal degradation and water resistance of intumescent coating, Appl. Clay Sci. 146 (2017) 350–361.
[22] A.M. Abdel-Gaber, B.A.A.-E. Nabey, E. Khamis, O.A. Abdelattef, H. Aglan, A. Ludwick, Influence of natural inhibitor, pigment and extender on corrosion of polymer coated steel, Prog. Org. Coat. 69 (2010) 402–409.
[23] K. Joncoux-Chabrol, J.-P. Bonino, M. Gressier, M.-J. Menu, N. Pébère, Improvement of barrier properties of a hybrid sol-gel coating by incorporation of synthetic talc-like phyllosilicates for corrosion protection of a carbon steel, Surf. Coat. Technol. 206 (2012) 2884–2891.
[24] E. Jubete, C.M. Liauw, N.S. Allen, Water uptake and tensile properties of carboxylated styrene butadiene rubber based water born paints: models for water uptake prediction, Prog. Org. Coat. 59 (2007) 126–133.
[25] C. Charnay, S. Lagerge, S. Partyka, Assessment of the surface heterogeneity of talc materials, J. Colloid Interface Sci. 233 (2001) 250–258.
[26] S. Petit, F. Martin, A. Wiewiora, P. De Parseval, A. Decarreau, Crystal-chemistry of talc: a near infrared (NIR) spectroscopy study, Am. Mineral. 89 (2004) 319–326.
[27] M. Sprynskyy, R. Gadzała-Kopciuch, K. Nowak, B. Buszewski, Removal of zearalenone toxin from synthetics gastric and body fluids using talc and diatomite: a batch kinetic study, Colloids Surf. B: Biointerfaces 94 (2012) 7–14.

[28] I.L. Lagadic, M.K. Mitchell, B.D. Payne, Highly effective adsorption of heavy metal ions by a thiol-functionalized magnesium phyllosilicate clay, Environ. Sci. Technol. 35 (2001) 984–990.
[29] Y. Meng, W. Xie, H. Wu, S.M. Tariq, H. Yang, Evolution of black talc upon thermal treatment, Minerals 12 (2022) 155.
[30] F.C. Ballotin, M. Nascimento, S.S. Vieira, A.C. Bertoli, O. Carmignano, A.P.D. C. Teixeira, R.M. Lago, Natural Mg silicates with different structures and morphologies: Reaction with K to produce K2MgSiO4 catalyst for biodiesel production, Int. J. Miner. Metall. Mater. 27 (2020) 46–54.
[31] W.-L. Qin, T. Xia, Y. Ye, P.-P. Zhang, Fabrication and electromagnetic performance of talc/NiTiO3 composite, R. Soc. Open Sci. 5 (2018), 171083.
[32] M. Świetlicki, D. Chocyk, T. Klepka, A. Prószyński, A. Kwaśniewska, J. Borc, G. Gładyszewski, The structure and mechanical properties of the surface layer of polypropylene polymers with talc additions, Materials 13 (2020) 698.
[33] Y. Cheng, G. Yu, B. Yu, X. Zhang, The research of conductivity and dielectric properties of ZnO/LDPE composites with different particles size, Materials 13 (2020) 4136.
[34] O.K. Mallem, F. Zouai, O.Y. Gumus, F.Z. Benabid, A.C. Bedeloglu, D. Benachour, Synergistic effect of talc/calcined kaolin binary fillers on rigid PVC: improved properties of PVC composites, J. Vinyl Addit. Technol. 27 (2021) 881–893.
[35] A.A. El-Midany, S.S. Ibrahim, The effect of mineral surface nature on the mechanical properties of mineral-filled polypropylene composites, Polym. Bull. 64 (2010) 387–399.
[36] K. Kalantari, M.B. Ahmad, K. Shameli, R. Khandanlou, Synthesis of talc/Fe3O4 magnetic nanocomposites using chemical co-precipitation method, Int. J. Nanomedicine 8 (2013) 1817.
[37] S. Sathiyanarayanan, R. Jeyaram, S. Muthukrishnan, G. Venkatachari, Corrosion protection mechanism of polyaniline blended organic coating on steel, J. Electrochem. Soc. 156 (2009), C127.
[38] M. Özcan, İ. Dehri, EIS study of the effect of high levels of SO 2 on the corrosion of polyester-coated galvanised steel at different relative humidities, Prog. Org. Coat. 44 (2002) 279–285.
[39] S.I. Bhat, S. Ahmad, Castor oil-TiO2 hyperbranched poly (ester amide) nanocomposite: a sustainable, green precursor-based anticorrosive nanocomposite coatings, Prog. Org. Coat. 123 (2018) 326–336.
[40] C. Hsu, F. Mansfeld, Concerning the conversion of the constant phase element parameter Y0 into a capacitance, Corrosion 57 (2001).
[41] B. Hirschorn, M.E. Orazem, B. Tribollet, V. Vivier, I. Frateur, M. Musiani, Determination of effective capacitance and film thickness from constant-phase-element parameters, Electrochim. Acta 55 (2010) 6218–6227.
[42] I. Thompson, D. Campbell, Interpreting nyquist responses from defective coatings on steel substrates, Corros. Sci. 36 (1994) 187–198.
[43] Y. González-García, S. González, R.M. Souto, Electrochemical and structural properties of a polyurethane coating on steel substrates for corrosion protection, Corros. Sci. 49 (2007) 3514–3526.
[44] J. Bisquert, A. Compte, Theory of the electrochemical impedance of anomalous diffusion, J. Electroanal. Chem. 499 (2001) 112–120.
[45] N. Arianpouya, M. Shishesaz, M. Arianpouya, M. Nematollahi, Evaluation of synergistic effect of nanozinc/nanoclay additives on the corrosion performance of zinc-rich polyurethane nanocomposite coatings using electrochemical properties and salt spray testing, Surf. Coat. Technol. 216 (2013) 199–206.
[46] R. Jagtap, R. Nambiar, S. Hassan, V. Malshe, Predictive power for life and residual life of the zinc rich primer coatings with electrical measurement, Prog. Org. Coat. 58 (2007) 253–258.
[47] R. Chaturvedi, R.K. Gupta, N.R. Gorhe, P. Tyagi, Percolative polyurethane-polypyrrole-straw composites with enhanced dielectric constant and mechanical strength, Compos. Part A Appl. Sci. Manuf. 131 (2020), 105810.
[48] J.L. Rosenholtz, D.T. Smith, The dielectric constant of mineral powders, Am. Mineral. 21 (1936) 115–120.
[49] D.M. Brasher, A.H. Kingsbury, Electrical measurements in the study of immersed paint coatings on metal. I. Comparison between capacitance and gravimetric methods of estimating water-uptake, J. Appl. Chem. 4 (1954) 62–72.
[50] M. Rodrıguez, J. Gracenea, J. Saura, J. Suay, The influence of the critical pigment volume concentration (CPVC) on the properties of an epoxy coating: part II. Anticorrosion and economic properties, Prog. Org. Coat. 50 (2004) 68–74.
[51] S.K. Singh, S.P. Tambe, G. Gunasekaran, V.S. Raja, D. Kumar, Electrochemical impedance study of thermally sprayable polyethylene coatings, Corros. Sci. 51 (2009) 595–601.
[52] N. Tang, W.J. van Ooij, G. Górecki, Comparative EIS study of pretreatment performance in coated metals, Prog. Org. Coat. 30 (1997) 255–263.
[53] M. Kendig, J. Scully, Basic aspects of electrochemical impedance application for the life prediction of organic coatings on metals, Corrosion 46 (1990) 22–29.
[54] B. Rotenberg, A.J. Patel, D. Chandler, Molecular explanation for why talc surfaces can be both hydrophilic and hydrophobic, J. Am. Chem. Soc. 133 (2011) 20521–20527.
[55] H. Elfaki, A. Hawari, C. Mulligan, Enhancement of multi-media filter performance using talc as a new filter aid material: mechanistic study, J. Ind. Eng. Chem. 24 (2015) 71–78.
[56] G.E. Morris, D. Fornasiero, J. Ralston, Polymer depressants at the talc–water interface: adsorption isotherm, microflotation and electrokinetic studies, Int. J. Miner. Process. 67 (2002) 211–227.
[57] G. Mälhammar, Determination of some surface properties of talc, Colloids Surf. 44 (1990) 61–69.
[58] H. Du, J. Miller, A molecular dynamics simulation study of water structure and adsorption states at talc surfaces, Int. J. Miner. Process. 84 (2007) 172–184.
[59] R.N. Wenzel, Resistance of solid surfaces to wetting by water, Ind. Eng. Chem. Res. 28 (1936) 988–994.
[60] A. Ghosal, O.U. Rahman, S. Ahmad, High-performance soya polyurethane networked silica hybrid nanocomposite coatings, Ind. Eng. Chem. Res. 54 (2015) 12770–12787.
[61] S. Pathan, S. Ahmad, Green and sustainable anticorrosive coating derived from waterborne linseed alkyd using organic-inorganic hybrid cross linker, Prog. Org. Coat. 122 (2018) 189–198.
[62] X. Yan, X. Qian, R. Lu, T. Miyakoshi, Synergistic effect of addition of fillers on properties of interior waterborne UV-curing wood coatings, Coatings 8 (2017) 9.
[63] R. Matsuzaki, N. Tsukamoto, J. Taniguchi, Mechanical interlocking by imprinting of undercut micropatterns for improving adhesive strength of polypropylene, Int. J. Adhes. Adhes. 68 (2016) 124–132.
[64] C.J.Ngally Sabouang, J.A. Mbey, Liboum, F. Thomas, D. Njopwouo, Talc as raw material for cementitious products formulation, J. Asian Ceram. Soc. 2 (2014) 263–267.